Pre-Charged Collapse-Mode Capacitive Micromachined Ultrasonic Transducer (CMUT) Receivers for Efficient Power Transfer

Saccher, Marta; Savoia, Alessandro Stuart; Van Schaijk, Rob; Klootwijk, Johan H.; Dekker, Ronald

DOI
10.1109/TUFFC.2024.3523179

Publication date
2024

Document Version
Final published version

Published in
IEEE Transactions on Ultrasonics, Ferroelectrics, and Frequency Control

Pre-Charged Collapse-Mode Capacitive Micromachined Ultrasonic Transducer (CMUT) Receivers for Efficient Power Transfer

Marta Saccher, *Member, IEEE*, Alessandro Stuart Savoia, *Member, IEEE*, Rob van Schaijk, Johan H. Klootwijk, *Senior Member, IEEE*, and Ronald Dekker

***Abstract*—Capacitive micromachined ultrasonic transducers (CMUTs) offer several advantages over standard lead zirconate titanate (PZT) transducers, particularly for implantable devices. To eliminate their typical need for an external bias voltage, we embedded a charge storage layer in the dielectric. The objective of this study was to evaluate the performance of plasma-enhanced chemical vapor deposition (PECVD) Si_3N_4 and atomic layer deposition (ALD) Al_2O_3 as materials for the charge storage layer and two different dielectric layer thicknesses, focusing on their application as receivers in a wireless power transfer link. Capacitance–voltage (*CV*) measurements revealed that Si_3N_4 has a higher charge storage capacity compared to Al_2O_3. Additionally, a thicker dielectric layer between the bottom electrode and the charge storage layer (B_{diel}) improved both charge trapping and retention, as assessed in dynamic accelerated lifetime transmit (TX)-mode tests. We then analyzed the power conversion performance of the fabricated CMUTs through both simulations and experiments. We performed extensive modeling based on an equivalent circuit derived from electrical impedance measurements of the fabricated CMUTs. The model was used to predict the power conversion efficiency under various conditions, including the charging field strength, the operating frequency, and parasitic series resistance. Power transfer experiments at 1- and 2.4-MHz recorded efficiencies exceeding 80% with an optimally matched load and up to 54% with a purely resistive load. Results confirmed that, with optimal load matching, the efficiency of different CMUT variants is comparable, indicating that the optimal variant should be selected based on additional criteria, such as charge retention time.**

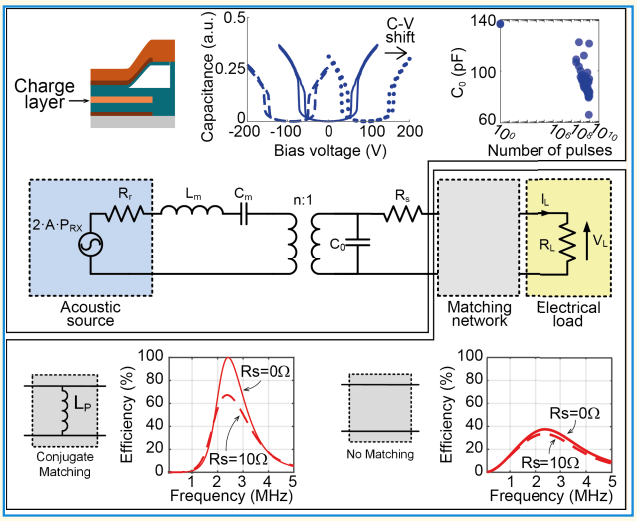

***Index Terms*—Capacitive micromachined ultrasonic transducers (CMUTs), implantable medical devices (IMDs), pre-charged CMUT, ultrasonic power transfer, zero-bias transducers.**

I. Introduction

IN RECENT years, new ultrasound markets have emerged to meet new customer demands, including continuous organ monitoring and handheld systems connectable to smartphones. Ultrasound transducers are now also considered as wireless power receivers for implantable medical devices (IMDs). However, traditional manufacturing processes, such as those using lead zirconate titanate (PZT) ultrasound transducers, have high manual labor costs and use toxic metals, limiting their suitability for certain applications.

Received 20 November 2024; accepted 16 December 2024. Date of publication 25 December 2024; date of current version 12 February 2025. This work was supported by the Electronic Components and Systems for European Leadership (ECSEL) Joint Undertaking Project Moore4Medical under Grant H2020-ECSEL-2019-IA-876190. *(Corresponding author: Marta Saccher.)*

Please see the Acknowledgment section of this article for the author affiliations.

Digital Object Identifier 10.1109/TUFFC.2024.3523179

An ultrasonically powered IMD platform includes a transmit (TX) transducer, medium, receive (RX) transducer, power management unit (PMU), and load. When designing an ultrasonically powered IMD, several critical factors must be considered. Key among these are the size of the device—particularly the RX size—the energy efficiency of the IMD, the RX sensitivity and bandwidth, and the biocompatibility and reliability [1].

The efficiency of the platform is crucial because low IMD efficiency requires transmitting higher power into the surrounding medium, which increases the risk of tissue damage. The overall efficiency of the IMD depends on the combined efficiencies of its components, especially the acoustic-to-electrical power conversion efficiency of the RX. Most research on ultrasonically powered IMDs still uses PZT crystals for the RX transducers, due to their efficiency ranging up to 60% [2], [3], [4], [5], [6], [7], thanks to

Highlights

- **Performance characterization of bias-free pre-charged collapse-mode CMUTs for power transfer applications obtained by embedding a charge storage layer (Si_3N_4 or Al_2O_3) in the dielectric.**
- **All tested charging electric fields produced collapse-mode devices showing promising charge retention, with power transfer simulations and experiments aligning and achieving more than 80% efficiency.**
- **Their CMOS compatibility and lack of external bias enable their use in implantable devices, imaging probes, patches, point-of-care devices, and ultrasound catheters, among others.**

their high electromechanical coupling coefficient [8], [9]. Micromachined ultrasonic transducers (MUTs), such as piezoelectric MUTs (PMUTs) and capacitive MUTs (CMUTs), are alternatives to PZT transducers. PMUTs use a thin-film piezoelectric layer, while CMUTs use electrostatic actuation. MUTs have larger bandwidths, are CMOS-compatible, and can be made biocompatible and miniaturized, addressing several key considerations in the design of ultrasonically powered IMDs. Recently, a few studies investigated the use of PMUTs as RX transducers in IMDs. However, the reported results show that they all suffer from low efficiency, due to their small electromechanical coupling coefficient [10], [11], [12], [13], [14].

In this article, we used CMUTs as RX. A CMUT consists of a membrane suspended over a vacuum gap. Through the vibration of this membrane, electrostatically actuated with an opposing electrode beneath the vacuum gap, ultrasound can be transmitted into, or received from the medium coupled to the membrane. CMUTs require an external dc bias voltage ranging between 50 and 100 V to bring the top membrane closer (noncollapse mode) or in partial contact (collapse mode) to the bottom dielectric. In addition, collapse mode operation increases the TX and RX sensitivity, and the output pressure up to three times compared to non-collapse mode [15], [16]. However, the need for an externally applied dc bias requires additional circuitry and limits miniaturizability. Moreover, the use of high voltages is not desirable for medical applications. To eliminate the need for an external bias voltage, special types of CMUTs can be fabricated with a charge-trapping layer embedded in their dielectric layer stack. By trapping enough charge, the device can be operated in collapse mode without the need for a dc bias. The concept of dielectric charging is not new; however, only a few groups investigated this concept applied to CMUTs [16], [17], [18], [19], [20], [21]. Dielectric charging, in fact, is usually seen as a reliability issue in MEMS devices since it causes instability of the device characteristics up to the point at which the device fails [22], [23], [24], [25]. The few groups that investigated pre-charged CMUTs, used SiO_2 or Si_3N_4 as material for the charging layer. However, most of them produced non-collapse-mode CMUTs, with the exception of Ho et al. [17], who used a low-frequency CMUT operating at 140 kHz. Choi et al. [20] compared the performance of Si_3N_4–SiO_2 and SiO_2 as charging layers, concluding that Si_3N_4 maintains its performance for a longer duration due to superior charge retention. It is evident from these studies that trapping sufficient charge to achieve a pre-charged collapse-mode CMUT is challenging, and the choice of material for the charge-trapping layer is crucial. Leveraging the fundamental concept of dielectric charging from the semiconductor memory industry, materials employed in this domain can be integrated into the CMUT dielectric as a charge storage layer to develop stable pre-charged collapse-mode CMUTs. In recent years, we conducted preliminary experiments with a high-frequency CMUT array (8-MHz center frequency) originally designed for imaging applications, incorporating an Al_2O_3 charge-trapping layer in its dielectric. The experiments demonstrated that these devices can trap a sufficient amount of charge to maintain collapse mode and deliver excellent acoustic performance and power conversion efficiency [26], [27]. We successfully used this array to create a B-mode image without the need for an external bias, utilizing a purely ac driving signal [28]. These promising results motivated us to develop a second generation of prechargeable CMUTs, designed for wireless power transfer at a lower frequency range.

The primary objective of this article is to investigate pre-charged collapse-mode CMUTs evaluating their performance and their suitability as candidates for replacing standard externally biased CMUTs or other ultrasonic transducers with a focus on their application as ultrasound receivers in IMDs. To achieve this, we evaluated the performance of plasma-enhanced chemical vapor deposition (PECVD) Si_3N_4 and atomic layer deposition (ALD) Al_2O_3 as materials for the charge storage layer in the dielectric of pre-charged collapse-mode CMUTs. Preliminary findings comparing the performance of Si_3N_4 and Al_2O_3 in terms of charge trapping, static charge retention, and acoustic-to-electric power conversion efficiency were presented in [29]. In this article, we expand on our previous work by examining the impact of varying thicknesses of the insulating layer beneath the charge storage layer and by analyzing charge retention in TX mode under different experimental conditions. In addition, in this work, we analyzed their power conversion performance both through simulations and experiments. Simulations were performed using an equivalent circuit model derived from the electrical impedance measurements of single-element pre-charged CMUT prototypes. These simulations quantified their efficiency using an optimal load under various operating frequencies, charging electric fields, and with or without matching networks. We considered both ideal conditions and nonideal characteristics, such as the presence of parasitic elements including the resistance introduced by electrical

interconnections on the chip. We conducted power conversion experiments on the fabricated prototypes to evaluate their efficiency. We then analyzed and discussed the simulation and measurement results to quantitatively assess the performance, correlating them with the practical aspects considered in this study.

II. Materials and Methods

A. CMUT Fabrication

The collapse-mode CMUTs used in this work were designed and fabricated with the aim to be used as ultrasonic power receivers. The microfabrication technology is based on a six-mask, low-temperature (<400 °C) sacrificial release process that uses CMOS-compatible materials. These CMUTs were designed for a two-way center frequency in immersion around 3 MHz and have a membrane diameter of 355 μm. The fabricated CMUTs consist of 173 membranes connected in parallel, occupying an area of 5 × 5 mm^2. Typically, these CMUTs are operated in collapse mode with a bias voltage of 120 V, significantly above the collapse voltage of ≈70 V. However, such a high dc bias cannot be used for power transfer in implantable devices. We, therefore, changed the standard CMUT architecture to eliminate the need for a bias voltage by replacing the bottom dielectric layer consisting only of SiO_2 with a stack including a charge storage layer.

The fabrication process of the CMUT begins with a silicon wafer provided with a PECVD oxide dielectric layer. Alternatively, an application-specified integrated circuit (ASIC) wafer with integrated electronics can be used. The bottom electrode, made of an aluminum alloy, is then deposited and patterned on top of the oxide layer [Fig. 1(a.i)]. Next, the charge storage layer (200-nm Al_2O_3 or Si_3N_4) is deposited on top of the bottom electrode sandwiched between two SiO_2 layers (120 or 200 nm below, and 60 nm above the charge storage layer). Subsequently, a sacrificial metal layer made of an aluminum alloy (mask 2) is deposited and patterned, which will later be removed by etching to create the vacuum-sealed cavity of the CMUT [Fig. 1(a.ii)]. A second dielectric layer (60-nm SiO_2) is deposited, followed by the deposition and patterning of the top electrode (mask 3) [Fig. 1(a.iii)]. The first part of the CMUT membrane (6-μm Si_3N_4) is then deposited [Fig. 1(a.iv)]. An etch hole is patterned on the side of the membrane (mask 4) to etch the sacrificial material and form the cavity [Fig. 1(a.v)]. This etch hole is then sealed by depositing the second part of the membrane in a low-pressure environment, creating the vacuum-sealed cavity [Fig. 1(a.vi)]. The total thickness of the Si_3N_4 membrane is 9 μm. The CMUT processing is completed by etching vias (mask 5) and patterning bond pads (mask 6) for contacting the top and bottom electrodes. Scanning electron micrograph (SEM) photographs and a schematic cross section of the fabricated devices showing different layers are shown in Fig. 1(b)–(d).

We designed and fabricated four-layer stack variants. Two variants were fabricated with ALD-deposited Al_2O_3 as the charge storage layer, and the other two with PECVD-deposited Si_3N_4. For each charge storage layer material, two different thicknesses of the SiO_2 dielectric layer in contact with the bottom electrode (B_{diel}) were used: one variant with a thickness of 120 nm, and the other with a thickness of 200 nm. Fig. 1(e) provides an overview of these variants, along with their respective names as referenced throughout this article.

To evaluate the dielectric breakdown of the CMUTs, we fabricated metal–insulator–metal (MIM) capacitors with dimensions of size 300 × 300 μm^2. MIM capacitors are structurally simpler yet effectively emulate the pull-in state of CMUTs. We included them in the mask design of the CMUTs; therefore, they have the same dielectric stack as they are exposed to the same processing steps. Accurate measurement of the breakdown field requires a known electrically active area, which is difficult to estimate for collapsed CMUTs because it changes continuously during a voltage sweep, making precise measurement almost impossible. In contrast, MIM capacitors have a predefined and stable area, simplifying breakdown field measurement and providing a reliable means of estimating the breakdown field for CMUTs.

B. I-V and CV Measurements

To determine the breakdown voltage of the MIM capacitors, we measured their current–voltage (I–V) curves. We used a Keithley 237 High Voltage Source/Measure Unit (Keithley Instruments, Cleveland, OH, USA), and linearly swept the voltage from 0 V until breakdown, with 1-V increments. We set the compliance current to 5 mA.

To minimize any alteration of the stored charge in our device, we employed a fast capacitance–voltage (CV) protocol with a voltage sweep rate of 80 V/ms. We superimposed a small ac signal of 81 MHz on a 200-Hz triangular wave varying between 0 and ±200 V. We used the change in the phase of the impedance when the CMUT goes in and out of collapse to draw the CV curve. Additionally, to further limit any change in the charge within the dielectric, we used two measurement protocols: a dc bipolar sweep between positive and negative voltages for uncharged devices, and a dc unipolar sweep of either only positive or negative voltages for devices charged with positive and negative polarities, respectively. We measured three samples for each experimental condition.

C. CMUT Precharging

In this study, we investigated the effects of charging the CMUT devices with different electric fields on the equivalent built-in voltage, the charge retention, and the power conversion efficiency. We pre-charged the CMUTs by applying electric fields ranging from 7.5 to 8.5 MV/cm, both with positive and negative polarities with respect to the bottom electrode. These parameters were selected based on results from our previous work, where we achieved stable pre-charged CMUTs by applying electric fields within this range [27], [30]. We applied each charging voltage to a pristine device for 5 min, where pristine indicates an uncharged and unmeasured device. In this work, the 5-min duration was selected arbitrarily, and a shorter charging time would still be sufficient to create a pre-charged collapse-mode device.

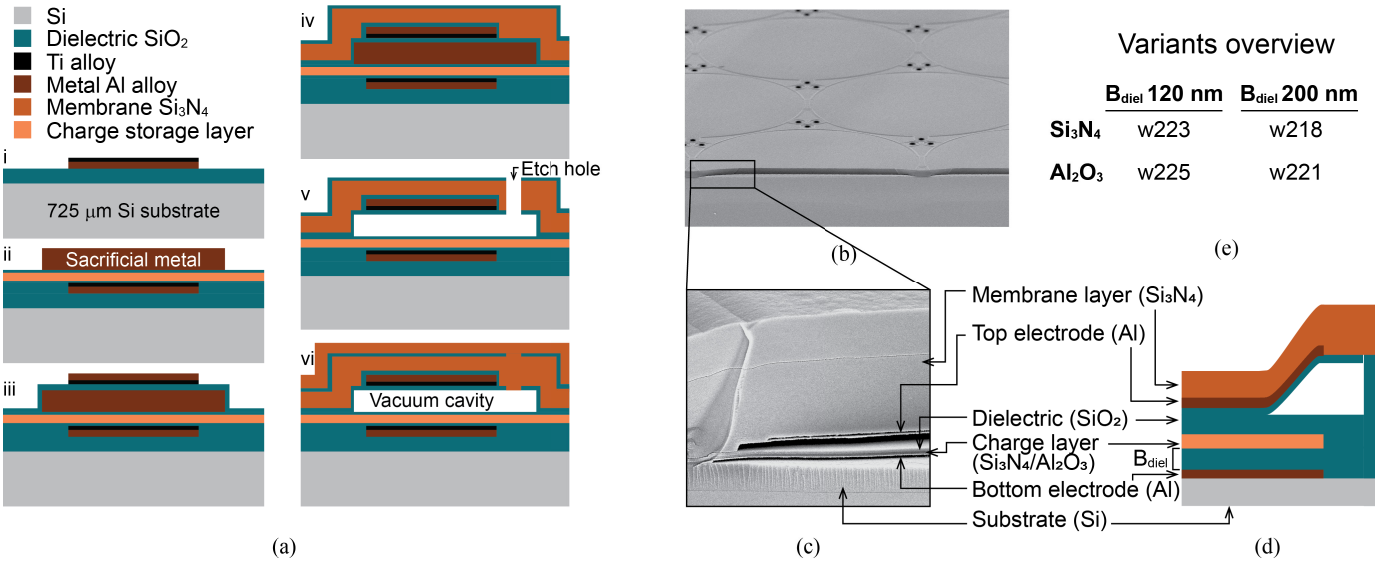

Fig. 1. (a) Schematic process flow of CMUT fabrication. (i) Bottom electrode deposition on top of oxide layer on Si substrate. (ii) Deposition of bottom dielectric layer stack including charge storage layer (Si_3N_4 or Al_2O_3), and deposition and patterning of the sacrificial metal. (iii) Deposition of second dielectric layer (SiO_2), and deposition and patterning of top electrode. (iv) Deposition of the first part of membrane layer. (v) Patterning of etch hole and removal via etching of the sacrificial metal to form the cavity. (vi) Sealing of the cavity in a low-pressure environment to form the vacuum gap by deposition of the second part of the membrane. The processing is finished with etching vias and patterning of bond pads for contacting top and bottom electrodes. (b) SEM photograph of a cross section of the fabricated CMUTs. (c) Magnification of SEM photograph highlighting the CMUT cell layers. (d) Schematic of the collapse-mode CMUT. (e) Overview of the fabricated variants with their respective names.

D. Charge Retention

Charge retention over time represents the major challenge for the pre-charged collapse-mode CMUTs, and it depends on the material of the dielectric layer, the deposition method, and the structure of the device. We performed three types of measurements to estimate the retention of the charge stored in the CMUTs. First, a static charge retention test, in which CMUT samples were not actively driven but underwent accelerated lifetime tests (ALTs) using temperature as an accelerating factor. Additionally, two other tests were conducted with the CMUTs operated in TX mode. In these tests, we monitored their impedance and output pressure, respectively, over the number of stimulation pulses. While this article primarily focuses on the use of pre-charged CMUTs in RX mode, we evaluated their performance in TX mode to explore their potential for other applications, such as imaging probes, wearable patches, or intravascular catheters.

1) Static: In these tests, the devices were not operated either in TX or RX mode; therefore, we could estimate the charge retention in conditions such as storage or periods of nonoperation. By performing multiple tests at different temperatures, the retention of the charge stored in the CMUTs can be estimated for the desired temperature (e.g., the body temperature of 37 °C). We used bare die CMUTs, pre-charged them with an electric field of −8 MV/cm for 300 s, and then placed them on a hotplate set at temperatures ranging from 140 °C to 160 °C. We programmed an impedance analyzer (Keysight E4990A, Keysight Technologies, Santa Rosa, CA, USA) to measure the CMUT impedance at regular intervals of time until the device failed. We defined the time to failure as when more than half of the CMUT membranes are out of collapse mode. This was determined using the method described in [27]. We repeated the test at least two times for each experimental condition.

2) Dynamic: For the impedance monitoring tests, we pre-charged bare die CMUTs with an electric field of −8 MV/cm for 300 s. We immersed them in Fluorinert and monitored their impedance over the number of stimulus pulses by using a Keysight E4990A impedance analyzer. To generate the stimulation pulses, we used a custom-made pulser board set to generate a two-cycle unipolar square wave burst at 2.6 MHz and 50% duty cycle, with a pulse repetition frequency of 100 kHz. We used the value of the equivalent blocked capacitance of the 173 cells composing the CMUTs, extrapolated from the measured impedance, to determine the number of cycles to failure, and we compared it to the value of the equivalent blocked capacitance at pull-in. This value is around 80 pF for all the CMUT variants, and it was used as a threshold to determine the charge retention of the devices. The test was repeated at least two times for each experimental condition.

For the output pressure monitoring tests, we mounted the CMUTs on a printed circuit board (PCB) and coated them with a thin layer of polybutadiene rubber (PBR). We charged them with an electric field of −7.5 MV/cm for 300 s. We then immersed them in a water tank filled with degassed water and centered a needle hydrophone (2762, Precision Acoustics, Dorchester, U.K.) at a distance of 3 mm from the CMUT surface to measure the output pressure. To generate the stimulation pulses, we used the same custom-made pulser board mentioned in the previous paragraph. For this experiment, we used a two-cycle bipolar square wave burst at 2.6 MHz and 50% duty cycle, with a pulse repetition frequency of 100 kHz.

E. Modeling and Experimental Analysis of Power Conversion

In an ultrasonic wireless power link, several critical elements are involved: the TX system, consisting of the driving

electronics, and an ultrasonic transducer capable of converting electrical power into acoustic power and radiating it into a propagation medium; the propagation medium, introducing attenuation phenomena such as diffraction, scattering, and absorption; and the RX system, comprising an ultrasonic transducer that converts acoustic power into electrical power, and conditioning electronics including circuits for the optimal transfer of the converted power to a load. As this study focuses on evaluating the performance of pre-charged CMUTs as transducer elements within the RX system, we have not considered the generation and propagation aspects of the system in our evaluations since these were extensively covered in existing literature. Our primary focus has been on the conversion of the acoustic power received by the CMUT into electrical power and its subsequent transfer to a load. For simplicity, we have considered a purely resistive linear electrical load and analyzed the conversion efficiency both without impedance matching and with a simple conjugate matching network to maximize power transfer.

Our analysis employed both modeling and experiments. The modeling accounted for the electromechanical characteristics of the pre-charged CMUT transducer, including its actual electrical impedance and the resulting electromechanical coupling, also comprising parasitic elements such as the series resistance of the electrical interconnections. We have conducted simulations to quantify the impact of the operating frequency and the interconnection parasitic resistance on power conversion efficiency, with and without the matching network. We, then, performed experiments on the four CMUT variants under different precharging conditions across a range of frequencies, and with and without the matching network. The simulation and experimental results were then contextually analyzed and discussed, providing a comprehensive understanding of the factors influencing power conversion efficiency in ultrasonic wireless power transfer systems.

1) CMUT Equivalent Circuit Model: To analyze the power conversion from the acoustic domain to the electrical domain, we used the equivalent circuit model of a pre-charged CMUT based on Mason's [31] model, as shown in Fig. 2(a). This model describes the electromechanical transduction through a two-port network comprising an electrical loop and a mechanical loop, coupled via a transformer with a turn ratio of 1:n. The electrical loop includes the blocked capacitance (C_0), while the mechanical loop includes the series combination of C_m and L_m, representing mechanical compliance and mass, respectively. The voltage in the mechanical loop represents the total force on the transducer surface, while the current represents the average velocity. The equivalent circuit also includes a series resistance (R_s) in the electrical port, representing the finite resistance of the CMUT's electrical interconnections, and a parallel resistance (R_r) in the mechanical port, representing the CMUT's radiation impedance. This equivalent circuit accurately represents the vibrating behavior around the fundamental mode of vibration of a spatially periodic layout of CMUT cells electrically connected in parallel and coupled to the propagation medium. It assumes that plane waves are radiated and received, which is valid if the pitch (the center-to-center distance between adjacent CMUT cells) is smaller than

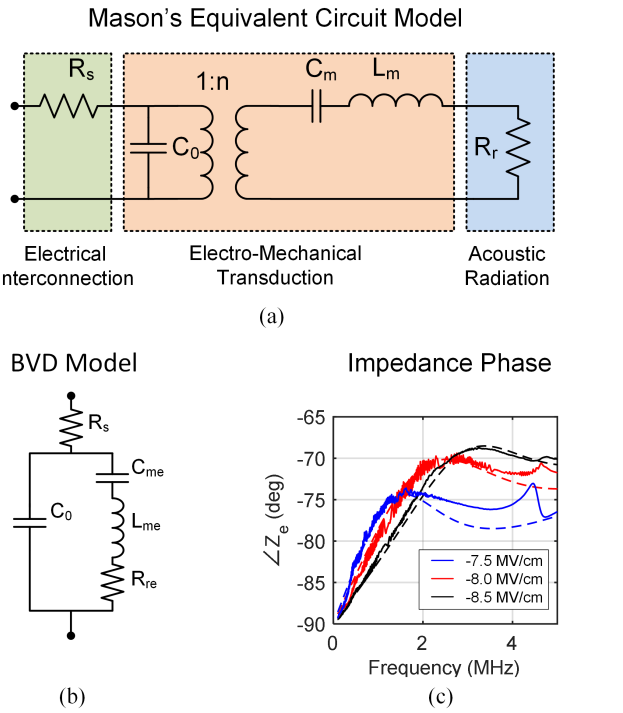

Fig. 2. Lumped-element CMUT equivalent circuit models: (a) Mason's model couples an electrical and a mechanical mesh using a transformer, and accounts for the acoustic radiation and the electrical interconnection using resistances; (b) BVD model represents the electrical impedance of the CMUT; and (c) measured and simulated electrical impedance phase of one of the fabricated CMUTs used in this work, charged at different electric fields.

the wavelength (or, in other words, for frequencies below the Bragg resonance frequency [32]) and if the CMUT aperture is large compared to the wavelength, thus justifying a purely real radiation impedance.

We derived the parameters of Mason's equivalent circuit model from the Butterworth–Van Dyke (BVD) model [33], [34] shown in Fig. 2(b). The BVD model was fit to the water-coupled pre-charged CMUT's electrical impedance measured with an impedance analyzer (Keithley E4990A, Keysight Technologies). We used MATLAB (MathWorks, Natick, MA, USA) to solve the optimization problem, constructing the model by converting the equivalent impedance of the BVD model into the s-domain and representing it with the *tf* function. We defined the objective function as the sum of the root mean square of the differences between the model and the measured impedance. This includes differences in the impedance when expressed both in the form of magnitude and phase, as well as in the form of real and imaginary parts. To minimize the objective function, we used the *fminsearch* function.

To extract Mason's equivalent circuit parameters from the BVD parameters, the following methodology was employed. First, the specific acoustic impedance of the medium (Z_m) and the acoustically active area of the transducer (A) were determined. Using these values along with the radiation resistance (R_{re}) from the BVD model, the electromechanical transformation ratio (n) was calculated as $n = ((Z_m \cdot A)/R_{\text{re}})^{1/2}$. This ratio ($n$) was then used to transform the BVD mechanical

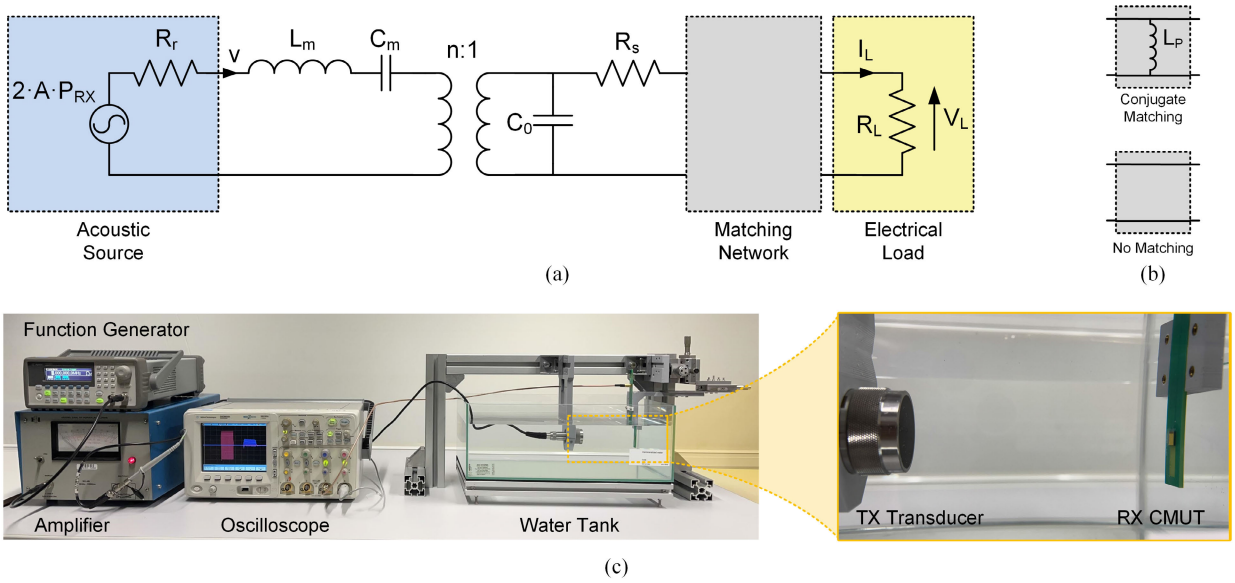

Fig. 3. (a) Equivalent circuit model used for the power transfer simulations. (b) Matching networks analyzed. (c) Experimental setup used for the power transfer experiments.

capacitance (C_{me}), inductance (L_{me}), and resistance (R_{re}) into Mason's parameters. Specifically, the mechanical compliance (C_m) is computed as (C_{me}/n^2), the mass (L_m) as $L_{\text{me}} \cdot n^2$, and the radiation resistance (R_r) as $R_{\text{re}} \cdot n^2$. The blocked capacitance (C_0) remained unchanged in both models. This systematic transformation allowed the parameters from the BVD model to be effectively translated into Mason's equivalent circuit model, enabling a more comprehensive description of the transducer's behavior when coupled to the propagation medium. We implemented the CMUT Mason's equivalent circuit model in LTSpice (Analog Devices, Norwood, MI, USA). As an example of the methodology effectiveness, we have reported in Fig. 2(c) the phase of the impedance of a prototype CMUT pre-charged at -7.5, -8, and -8.5 MV/cm, and measured and calculated using the LTSpice model, demonstrating a good agreement between the numerical and experimental data. The measured and simulated curves show good agreement in the lower frequency range up to the first peak, where the CMUT vibrates around the fundamental mode. For higher frequencies, the agreement is less accurate as the CMUT vibrates around the second axis-symmetric mode, which the model does not account for. However, the discrepancy remains minor at low charging field values, such as -7.5 MV/cm, and is practically negligible at higher field values within the frequency range of interest.

2) Optimal Load Computation: As mentioned, we analyzed the power transfer from the CMUT to an optimal load with and without using an impedance-matching network. As known, the condition for maximum power transfer from a generator to a load is achieved when the equivalent source impedance, i.e., the Thevenin impedance, and the load impedance are complex conjugates. The impedance of a water-coupled pre-charged CMUT (Z_e), including R_s, typically consists of a resistance and a capacitive reactance. Therefore, for the case with a matching network, we used a matching inductor L_P and an optimal load resistor R_L connected in parallel to the CMUT electrical port, dimensioned in such a way as to achieve conjugate matching using the following equations:

$$R_L = \frac{X_e^2 + R_e^2}{R_e} \tag{1}$$

$$L_P = -\frac{X_e^2 + R_e^2}{2\pi f_m X_e} \tag{2}$$

where R_e and X_e are the real and imaginary parts of Z_e, respectively, and f_m is the matching frequency. It should be noted that other matching network configurations are possible, and depending on the application, one can be more suitable than another. Here, the parallel configuration was chosen as there were no specific requirements on the load, such as specific voltage or current ranges, and it was the easiest to implement in this case. However, any chosen matching configuration will include an inductor to compensate for the capacitive reactance of the CMUT introduced by the relatively large blocked capacitance and the relatively low mechanical quality factor in immersion. For the case without matching, we calculated the optimal load as a purely resistive load, for which the maximum power transfer is achieved when the load resistance R_L is equal to the magnitude of the fluid-coupled CMUT impedance $|Z_e|$. A derivation of the maximum power transfer condition for the case without matching is presented in the Appendix.

3) Power Transfer Simulations: We conducted power transfer simulations using the circuit model shown in Fig. 3(a), which is implemented in LTSpice. The model includes an acoustic source connected to the mechanical port of the CMUT Mason's equivalent circuit model, which represents the force exerted on the surface of a CMUT with area A by an impinging pressure wave with amplitude P_{RX}. A series resistance R_s, a matching network, and a load resistance R_L are connected to the CMUT model electrical port. Fig. 3(b) schematically

TABLE I
MASON'S MODEL PARAMETERS

Efield (MV/cm)	**−7.5**	**−8.5**
$\mathbf{C_0}$ (pF)	547	696
$\mathbf{C_m}$ (nm/N)	5.3	1.9
$\mathbf{L_m}$ (μH)	2.9	1.9
$\mathbf{R_r}$ (g/s)	37	37
n (mN/V)	189	316

illustrates the two matching scenarios considered, i.e., *Conjugate Matching* and *No Matching*. We chose to model the Si_3N_4 CMUT with 200-nm B_{diel} thickness design variant, charged at two electric field values, −7.5 and −8.5 MV/cm, and analyzed its performance for three values of R_s: 0, 5, and 10 Ω. The resistance values were chosen based on the consideration that the series resistance determined from the fitting of the electrical impedance data measured on the fabricated CMUTs is in the order of 10 Ω. First, we calculated the electrical impedance of the CMUT for the two charging fields and $R_s = 0$ Ω. Then, from their impedance phase curves, we identified the frequencies f_L and f_H, which refer to the frequencies at which the phase of the CMUT charged with an electric field of −7.5 and −8.5 MV/cm is, respectively, minimum. For the *Conjugate Matching* case, we calculated the values of R_L and L_P for the six combinations of charging field and R_s at f_L and f_H, which function as matching frequency f_m. For the *No Matching* case, for each charging field variant, we calculated the value of R_L at their respective minimum phase frequency for the three R_s values. The CMUT Mason's equivalent circuit model parameters for the two charging field variants are reported in Table I.

For all considered cases, we performed an ac analysis over a frequency range from 100 kHz to 4 MHz, applying an arbitrary pressure P_{RX} of 1 Pa and calculating the current I_L and voltage V_L across the load R_L. We, then, calculated the received acoustic power as $W_a = ((A \cdot P_{RX}^2)/(2 \cdot Z_m))$, where Z_m is the specific acoustic impedance of the medium, and the electrical power dissipated by the load as $W_e = (1/2)\Re\{V_L \cdot \text{conj}(I_L)\}$, from which we finally derived the power conversion efficiency $\eta = (W_e/W_a)$ as a function of frequency. In all the simulations, we considered a Z_m of 1.48 MRayl to model the CMUT operation in water coupling conditions.

4) Power Transfer Experiments: We evaluated the power conversion efficiency of the four pre-charged CMUT variants through ultrasonic power transfer experiments. We used commercial single-element circular immersion transducers (Olympus NDT Inc., Waltham, MA, USA) as TX transducers. We evaluated the performance at 1 and 2.5 MHz, using a 25-mm-diameter TX transducer (Olympus V302S-SU) and a 39-mm-diameter TX transducer (Olympus V395S-SU), respectively. The RX transducers were the pre-charged CMUTs. To determine the optimal distance for maximum power at the RX transducer, we conducted ultrasound field simulations using FOCUS [35]. Based on the simulation results, we performed experiments at 1 MHz with a distance of 110 mm between the TX and RX transducers, and at 2.5 MHz with a distance of 215 mm. Before conducting the power transfer experiment, we measured the pressure field generated by the TX transducer at these distances. This was done by scanning a plane parallel to the surface of the transducer using a needle hydrophone (2762, Precision Acoustics). For the power transfer experiment, both the TX and RX transducers were immersed in a water tank and centrally aligned.

Fig. 3(c) shows the setup used for the power transfer experiments. The driving signal for the TX transducer was generated by a function generator (Agilent 33250A, Agilent Technologies, Santa Clara, CA, USA) and amplified by an RF amplifier (ENI 240L, Electronics and Innovation, Rochester, NY, USA). An oscilloscope (Agilent DSO6034A) was used to measure the input signal to the TX transducer and measure the output voltage from the CMUTs under test. For this experiment, the CMUTs were mounted on a PCB and coated with a thin layer of PBR. We attached the CMUTs PCB to a custom-made 3-D printed holder connected to micromanipulators that allowed the adjustment of the position in the x-, y-, and z-directions.

We conducted the power transfer experiment for each CMUT type and charging electric field. We drove the TX transducers using a 20-cycle sine burst with a pulse repetition frequency of 10 Hz. The acoustic pressure amplitude at the surface of each RX transducer was 114 kPa at 1 MHz and 98.5 kPa at 2.4 MHz, corresponding to an intensity of approximately 420 and 300 mW/cm^2, respectively. These values were about half of the Food and Drug Administration (FDA) limit of 720 mW/cm^2 for safe use of ultrasound in the human body [36]. We obtained these values from the acoustic characterization of the TX transducers. For each CMUT type and charging electric field, we determined the values of the matching network and optimal load components from the CMUT equivalent impedance, for both the *Conjugate Matching* and *No Matching* cases. The matching components consisted of single inductors with a high-quality factor (RF Chokes, BC+/LBC+ Series, EPCOS AG, Munich, Germany) and a precision potentiometer (Bourns, Riverside, CA, USA).

III. RESULTS AND DISCUSSION

A. I-V and CV Measurements

Fig. 4(a) shows the results of the I–V measurements in the form of current density–electric field (J–E) curves. Comparing the curves of the Si_3N_4 samples to the ones of Al_2O_3, it can be observed that the current density (J) of Si_3N_4 samples is slightly higher than that of the Al_2O_3 ones and that the curves exhibit similar trends for devices with the same material, independently of B_{diel} thickness. Moreover, the current density is not perfectly symmetric for electric fields of positive and negative polarities, and the breakdown field of Si_3N_4 is slightly higher than the that of Al_2O_3. Specifically, the Al_2O_3 samples have a breakdown field around 8–8.5 MV/cm, while the breakdown of Si_3N_4 samples is between 8.5 and 9.5 MV/cm. Additionally, the two dielectric materials show different J–E curve shapes, with Al_2O_3 showing a gradual rise in current from above 5 MV/cm followed by a narrow region of fast charging above 7.5–8 MV/cm before breakdown, while Si_3N_4 shows a more gradual increase in current before breakdown. These findings align with the trends observed in

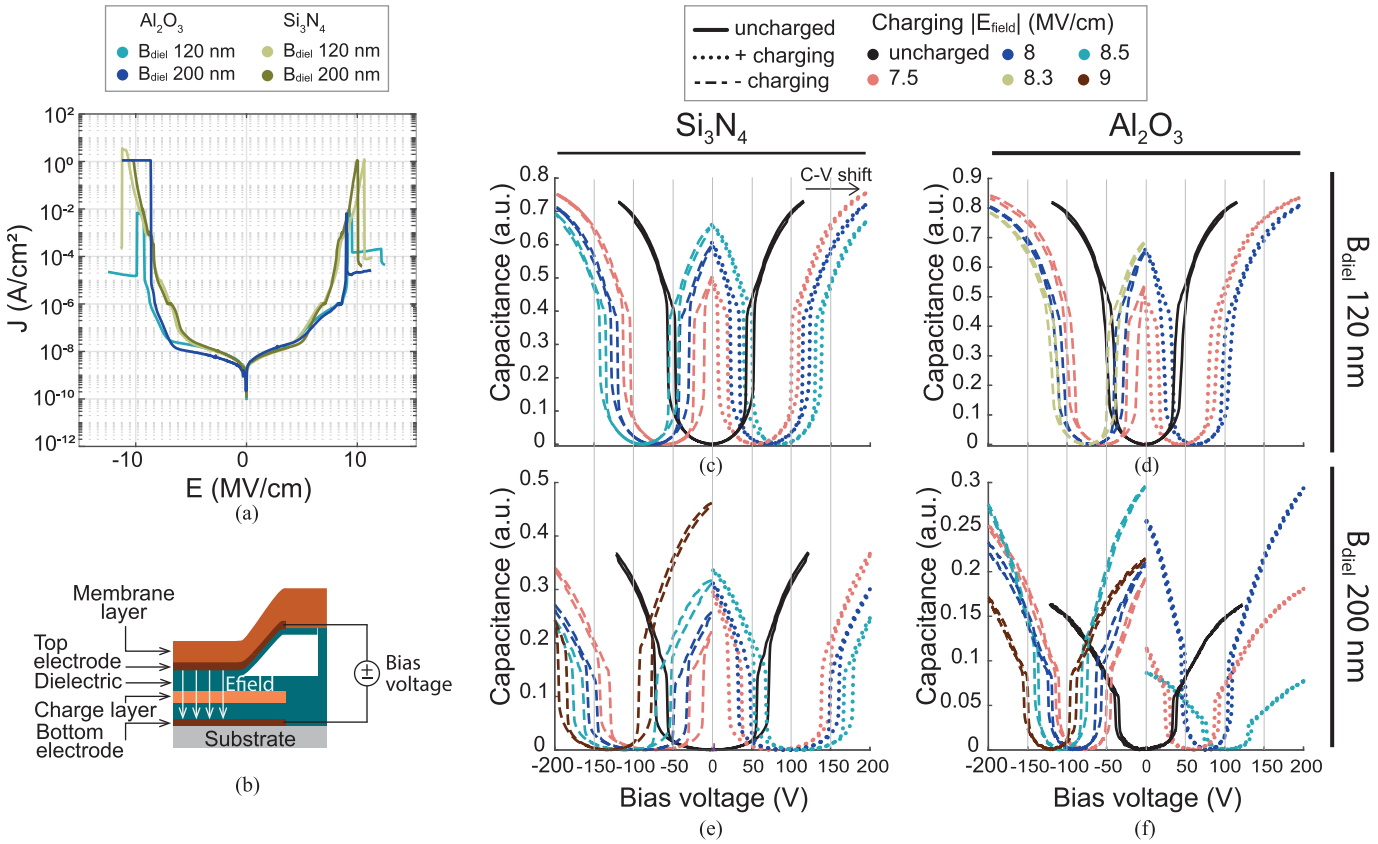

Fig. 4. (a) *J–E* curves of fabricated MIM capacitors with Al_2O_3 and Si_3N_4. (b) CMUT schematic during charging with positive polarity illustrating the direction of the electric field. (c) and (e) Comparison of *CV* curve shift for Si_3N_4 samples with B_{diel} of 120 and 200 nm, respectively, when charged with different electric fields and polarity. (d) and (f) Same as (c) and (e) but for Al_2O_3.

other research [27], [37] and are due to different transport mechanisms in Si_3N_4 and Al_2O_3. Identifying the exact charge transport mechanisms of electrons is, however, beyond the scope of this work.

Fig. 4(c)–(f) shows the *CV* curves of the four CMUT variants charged with different electric fields. The *CV* curve of the pristine devices exhibits symmetry around 0 V. In addition, 0 V coincides with the point of minimum capacitance, indicating that the CMUT is not in a collapsed state and has no charge stored in the dielectric. On the other hand, the pre-charged devices show a shift in the point of minimum capacitance of 60–100 V. The pull-in and snap-out points are beyond 0 V, indicating that the CMUT is in a collapsed state even at 0-V bias, and the presence of charge in the dielectric. Moreover, as expected, the shift is larger for higher charging electric fields due to a larger amount of charge stored in the dielectric. We summarized the shift in collapse voltage due to the charge stored in different CMUT variants in Table II.

Fig. 4 shows that charging the Al_2O_3 devices with B_{diel} of 120 nm with an electric field exceeding 8 MV/cm was only feasible with negative polarity, as devices charged with positive polarity experienced dielectric breakdown. An analogous behavior can be observed for the Si_3N_4 and Al_2O_3 devices with 200-nm B_{diel}, as charging with an electric field of 9 MV/cm could only be achieved with an electric field of negative polarity. Slight asymmetries arising from the fabrication process due to the influence of the underlying material on each deposited layer can explain these results and the asymmetries observed in the *I–V* curves in Fig. 4(a).

TABLE II
SUMMARY OF THE SHIFT IN MINIMUM CAPACITANCE VOLTAGE EXTRACTED FROM THE *CV* MEASUREMENTS

B_{diel} (nm)			Charging Efield (MV/cm) −8.5	−8	−7.5	7.5	8	8.5
120	Si_3N_4		-91.7	-77.1	-59.9	59.8	74.7	90.7
	Al_2O_3		-	-68.7	-53.4	48.6	66.7	-
200	Si_3N_4		-114.8	-94.8	-76.6	85.2	97.1	116.1
	Al_2O_3		-106.7	-90.2	-79.8	58.5	78.2	91.4

Additionally, comparing the *CV* shift for the two B_{diel} thicknesses, the 200-nm variants show a larger shift compared to the thinner B_{diel}, indicating that more charge is stored. Moreover, the effect of the charging electric field polarity is nearly the same for all four variants. An exception is the Si_3N_4 variant with 200-nm B_{diel} which shows, although minimal, an opposite trend. However, this could be due to some imprecision in the measurement or inherent variations between samples, and the magnitude of the difference remains small. A larger amount of stored charge implies a higher equivalent built-in bias voltage, with two main consequences: a shift in the device's resonant frequency toward higher values [38] and a longer lifetime, which is discussed in Section III-B.

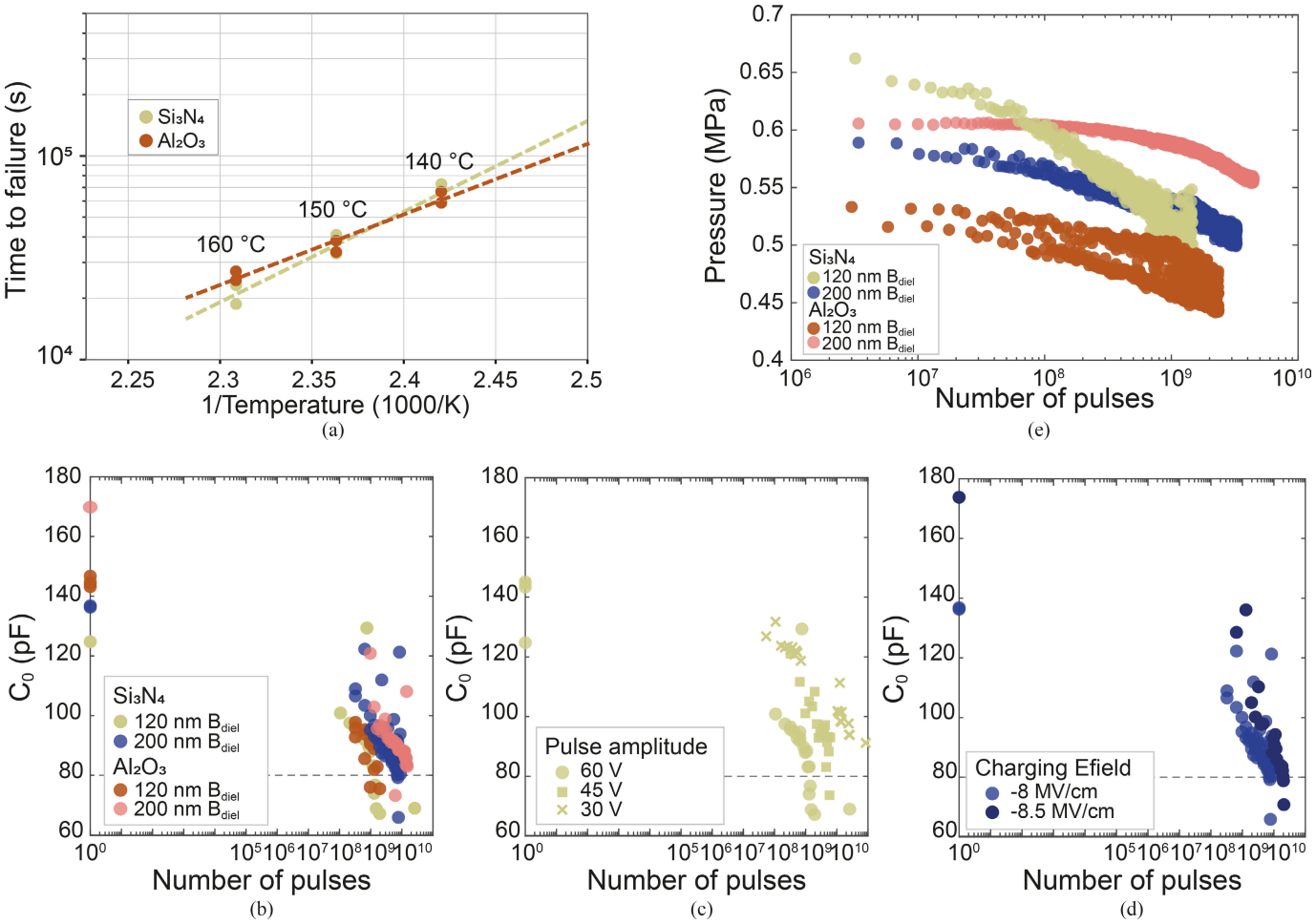

Fig. 5. Accelerated lifetime measurement results. (a) Fitting of the results from the static ALT measurements for the 120-nm Al_2O_3 and Si_3N_4 tested samples. Dynamic charge retention results from impedance monitoring tests. (b) Comparison of electrical capacitance (C_0) over the number of stimulus pulses during dynamic ALT for the four tested variants. Results for unipolar stimulus with 60-V amplitude. (c) Effect of unipolar stimulus amplitude on (C_0) of 120-nm tetraethylorthosilicate (TEOS) Si_3N_4 samples. (d) Effect of charging electric field on (C_0) of 200-nm TEOS Si_3N_4 samples when stimulated with unipolar pulses with 60-V amplitude. (e) Output pressure over the number of stimulus pulses for dynamic ALT with bipolar pulses of 45-V peak-to-peak amplitude for the four CMUT variants.

Ultimately, both the Si_3N_4 variants exhibit a larger shift in the CV curve compared to the Al_2O_3 ones for both polarities. The average trap density of Si_3N_4 is in fact one order of magnitude larger than Al_2O_3 ($\approx 10^{-3}$ versus 10^{-4} C/m^2) [39], [40], [41].

These results confirm that the CMUTs must be charged with electric fields in the region of high current increase [Fig. 4(a)] to achieve a collapse-mode device. This finding is consistent with our observations in previous work [27]. In addition, they suggest that using a thicker B_{diel} and Si_3N_4 as material for the charge storage layer is beneficial in obtaining devices with a larger amount of stored charge. Yet, even more important than the ability to trap charge is the ability to retain it over time and over the device operation.

B. Accelerated Lifetime Measurements

1) Static: These measurements only provide a general estimation of the charge retention associated with the use of Si_3N_4 or Al_2O_3 in the dielectric stack. Therefore, we only tested the two device variants with B_{diel} of 120 nm. Fig. 5(a) presents the experimental results, fit to extrapolate the devices' charge retention at lower temperatures, showing that the predicted charge retention of the Si_3N_4 variant is longer than for the Al_2O_3 variant. At the body temperature of 37 °C, the predicted static charge retention is about 7.8 years for the Si_3N_4 variant and 1.2 years for the Al_2O_3 variant. However, this charge retention prediction is based on the fitting of an exponential relationship; therefore, small variations in time to failure at high test temperatures will result in large variations in estimated charge retention at lower temperatures such as body or ambient temperature. In addition, at high temperature, the devices' mechanical characteristics can vary significantly, and failure mechanisms other than charge detrapping may also be accelerated compared to as they occur in actual operation conditions. Nevertheless, despite the possibility that these experimental conditions may have degraded the performance of the CMUTs, the results are promising and indicate that the charge is not immediately detrapped.

2) Dynamic: Fig. 5(b) shows the comparison of the performance of the four CMUT variants in terms of the decrease in equivalent electrical capacitance C_0 when subjected to unipolar voltage amplitudes of 60 V. This amplitude is one of the

maximum used in standard CMUTs during transmission. The comparison is based on the number of pulses required for C_0 to reach the threshold value of 80 pF, which corresponds to the capacitance at pull-in. For the samples with 120-nm B_{diel}, the Al_2O_3 variant requires slightly more pulses to reach this threshold than the Si_3N_4 variant, indicating a longer charge retention. A similar pattern is observed for the samples with a 200-nm B_{diel} layer, where the Al_2O_3 variant again outperforms the Si_3N_4 variant.

We, then, tested the effect of different unipolar pulse amplitudes on the charge retention of the Si_3N_4 variant with 120-nm B_{diel}. Fig. 5(c) shows the comparison of the effect of unipolar pulses ranging from 30 to 60 V. As expected, lowering the pulse amplitude significantly increases the charge retention since the electric field generated by the external pulses affects the charge distribution in the CMUT dielectric.

Next, we tested the effect of charging the CMUTs with different electric fields. The CV measurements indicated that higher electric fields during charging lead to more charge being stored in the device. To investigate whether this increased charge storage translates into a longer retention, we compared the charge retention of Si_3N_4 samples with 200-nm B_{diel} when charged with electric fields of -8 and -8.5 MV/cm. Fig. 5(d) confirms that charging the device with a higher electric field results in a longer charge retention.

Finally, Fig. 5(e) illustrates the decrease in output pressure over the number of stimulation pulses for the four CMUT variants. Considering a threshold of 10^9 pulses, a value typically used for the qualification of ultrasound probes produced for point-of-care applications [25], the Al_2O_3 samples with a 200-nm B_{diel} layer show the best performance with only a 6.6% drop at the threshold of 10^9 cycles. The Si_3N_4 samples with a 200-nm B_{diel} layer showed a decrease in the output pressure of 10%, followed by the devices with the thinner B_{diel} layer: Al_2O_3 and Si_3N_4 experienced drops of 13.2% and 22.7%, respectively. The significant decrease in output pressure for the Si_3N_4 sample could be attributed to pre-existing degradation in the sample, as the pressure drop is expected to be similar to that of the Al_2O_3 version, considering the results shown in Fig. 5(b).

The results achieved by monitoring the CMUTs' impedance and output pressure show similar trends although a direct comparison between these measurements is challenging. The results here obtained can be used to define the range of applications for which these pre-charged CMUTs can be used. The decrease in electrical capacitance and therefore output pressure over time corresponds to a performance degradation as the CMUT cells gradually snap back to the non-collapsed state. This is advantageous compared to standard externally biased devices, where a short circuit in one cell can abruptly impact the dc bias of other cells, leading to sudden failure of the entire array. Furthermore, charging the devices with a higher electric field does not seem to induce dielectric degradation, as the performance degradation of the devices in Fig. 5(d) follows a similar trend. Moreover, the results from the static charge retention are contradictory to the ones of the dynamic charge retention as, in the former, Si_3N_4 samples showed longer charge retention prediction compared to Al_2O_3. However, as mentioned earlier, the static charge retention measurements are based on the fitting of an exponential relationship. Therefore, small measurement errors at the high test temperatures could have affected the estimated charge retention at a much lower temperature. Additionally, high temperatures could have elicited different discharge mechanisms in the two different materials.

Overall, these preliminary tests show promising performance. However, additional tests need to be performed to assess the charge retention of the devices. Reliability is a statistical process, so testing a larger number of samples will be necessary to obtain an accurate estimation of their charge retention. Furthermore, the CMUTs were exclusively tested in TX mode. Future tests in RX mode should be conducted to evaluate their charge retention in this mode. This will provide a more comprehensive understanding of their performance across different operational modes.

C. Power Conversion

1) Power Transfer Simulations: Fig. 6(a) and (b) shows the magnitude and phase of the simulated electrical impedance for the CMUTs charged at -7.5 and -8.5 MV/cm for $R_s = 0\ \Omega$. The magnitude curves indicate that the CMUT charged at -8.5 MV/cm has a generally lower impedance than the one charged at -7.5 MV/cm. This is because it is in a deeper collapse condition, where a larger portion of the CMUT membrane is in contact with the substrate. The phase curves show that the frequency at which the phase is minimum for the CMUT charged at -7.5 MV/cm is $f_L = 1$ MHz, while for the CMUT charged at -8.5 MV/cm is $f_H = 2.4$ MHz. This difference is due to the resonance frequency's dependence on the bias condition. The CMUT charged at -8.5 MV/cm has a higher resonance frequency because of the smaller vibrating portion of the CMUT membrane. The respective impedance phase values are substantially the same, approximately $-76.6°$. Thus, within the conditions analyzed in this article, the charging field of the CMUT mainly affects the magnitude of the electrical impedance and the central operating frequency without significantly altering the electromechanical coupling.

Fig. 6(c) and (d) presents the power conversion simulation results for the *Conjugate Matching* case with matching frequencies f_m equal to f_L (1 MHz) and f_H (2.4 MHz), respectively, while Fig. 6(e) shows the results for the *No Matching* case. Each graph shows the efficiency as a function of frequency for the two charging field cases and, for each, the three considered R_s values. The efficiency curves for the *Conjugate Matching* case show that maximum efficiency is achieved at f_m and it reaches 100% for $R_s = 0\ \Omega$, while it visibly decreases as R_s increases. Moreover, for each charging field case, the power bandwidth is greater when f_m is close to the respective frequency at which the phase is minimum. In this condition, for $R_s = 0\ \Omega$, the fractional power bandwidth at -3 dB is around 52% for both charging field cases. On the other hand, the bandwidth reduces when f_m is far from the minimum phase frequency. For the *No Matching* case, the efficiency is highest at the minimum phase frequency, and for $R_s = 0\ \Omega$, it reaches around 37.5% for both charging field

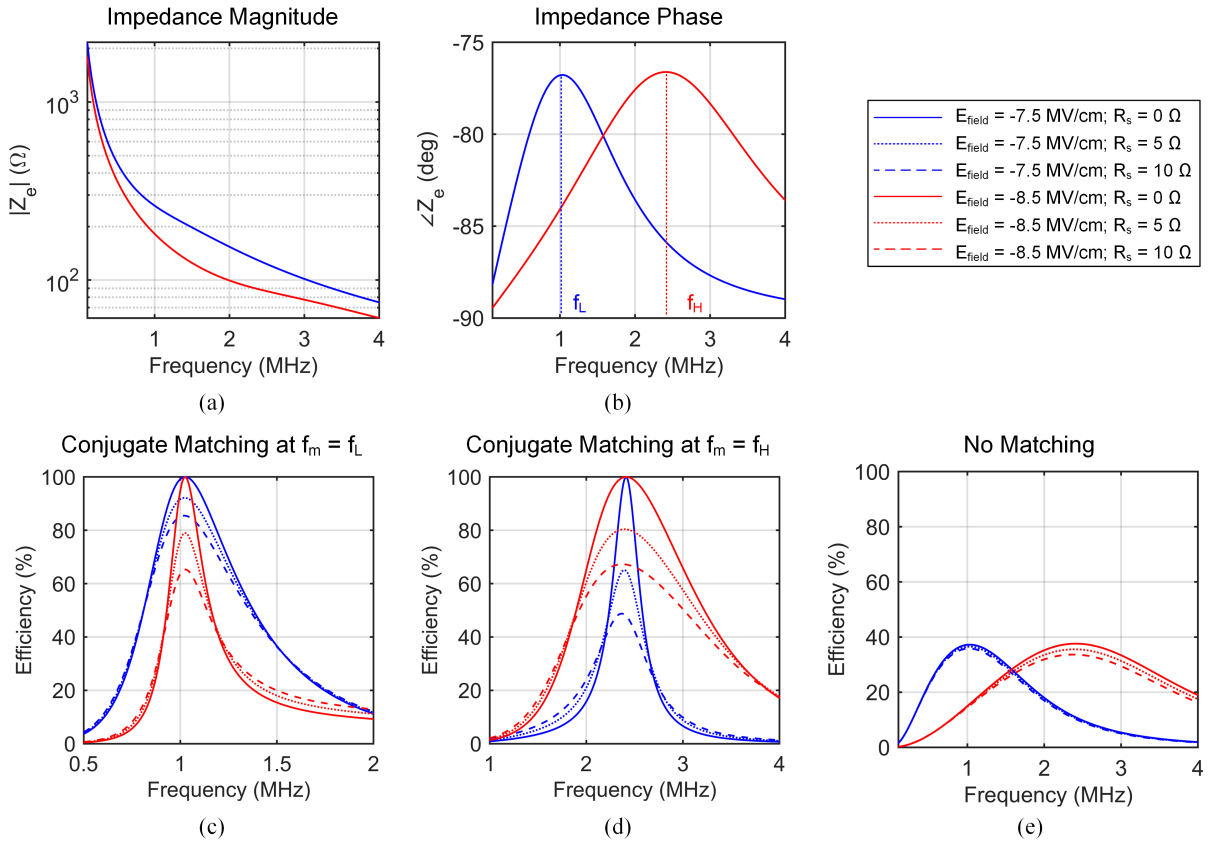

Fig. 6. Simulated electrical impedance (a) magnitude and (b) phase of the two CMUT charging field variants. Simulated power conversion efficiency in the *Conjugate Matching* case for (c) $f_m = f_L$ and (d) $f_m = f_H$, and (e) in the *No matching* case. The blue and red curves are related to charging fields of -7.5 and -8.5 MV/cm, respectively, while the line style is related to different R_s cases considered.

TABLE III
SUMMARY OF ULTRASONIC POWER TRANSFER EXPERIMENTAL RESULTS FOR THE TESTED DEVICES

		B_{diel} 120 nm						B_{diel} 200 nm					
		Si_3N_4 (w223)			**Al_2O_3** (w225)			**Si_3N_4** (w218)			**Al_2O_3** (w221)		
	Charging Efield (MV/cm)	−7.5	−8	−8.5	−7.5	−8	−8.5	−7.5	−8	−8.5	−7.5	−8	−8.5
1 MHz	**Power Conjugate Matching** (mW)	46.1	39.1	39.1	40.5	41.3	41.5	41.4	42.7	33.8	63.1	16.6	19.7
1 MHz	η **Conjugate Matching**	42.9%	36.4%	36.4%	37.7%	38.4%	38.7%	38.5%	39.7%	31.4%	58.8%	15.5%	18.3%
1 MHz	**Power No Matching** (mW)	21	17.9	17.6	16.2	18.9	18.4	18.2	19.2	–	29.3	6.9	7.2
1 MHz	η **No Matching**	19.5%	16.7%	16.4%	15.1%	17.6%	17.1%	16.7%	17.9%	–	27.3%	6.4%	6.7%
2.5 MHz	**Power Conjugate Matching** (mW)	20.7	28.1	62.5	21.8	24.3	46	19.9	24.6	48.8	39.6	62.1	66
2.5 MHz	η **Conjugate Matching**	27.2%	36.9%	82.0%	28.4%	31.9%	60.4%	26.1%	32.3%	64.0%	52.0%	81.6%	86.6%
2.5 MHz	**Power No Matching** (mW)	10.1	16.6	39.5	8.4	12.4	28.8	8.7	13.2	28.6	18.4	34.2	41.5
2.5 MHz	η **No Matching**	13.2%	21.8%	51.9%	11.0%	16.2%	37.9%	11.4%	17.3%	37.5%	24.1%	44.9%	54.5%

cases. In this condition, the efficiency decrease as a function of R_s is less pronounced than in the *Conjugate Matching* case. The fractional power bandwidth at -3 dB is much broader in the *No Matching* case, being 130% and 110% for charging fields of -7.5 and -8.5 MV/cm, respectively.

2) Power Transfer Experiments: We performed the first series of power transfer experiments connecting an optimally matched load consisting of L_P parallel to R_L to each of the pre-charged CMUT variants, and we summarized the results obtained in Table III. The results indicate that there is no absolute optimal device variant in terms of power transfer efficiency. Most of the devices charged with electric fields of -7.5 MV/cm have a better performance at 1 MHz compared to 2.4 MHz. On the other hand, devices charged at -8.5 MV/cm have a better performance at 2.4 MHz, reaching efficiencies up to 80%. This is in line with the simulation results in Fig. 6(c) and (d). We then repeated the previous experiment by connecting a purely resistive load to the CMUT (*No Matching* condition). As for the previous experiments, the results in Table III show no absolute optimal device variant. The charging electric fields for which different devices variants show the highest efficiency at the two test frequencies are the same that exhibited the highest efficiency when connected to the *Conjugate Matching* load. Also, in this case, these results are consistent with the simulation results presented in Fig. 6(e).

A comparison of the simulation and experimental results shows that, despite some variability in the measured efficiency values, there is excellent agreement at high frequency (2.4 MHz) for the -8.5-MV/cm charging field in both the *Conjugate Matching* and *No Matching* cases, as well as for the -7.5-MV/cm charging field, especially in the *No Matching*

TABLE IV
PERFORMANCE SUMMARY OF THE ULTRASONIC RECEIVER AND COMPARISON WITH THE STATE OF THE ART

Ref.	Material	Topology	Dimensions	Thickness	$\mathbf{f_m}$[MHz]	$\mathbf{W_e}$[mW]	η
[42]	PZT	disk	25 mm diameter	-	0.84	62.5	35 %
[43]	PZT	disk	30 mm diameter	2 mm	1	2.1	20 %
[2]	PZT	rectangular	2×4 mm^2	2 mm	1.15	12	2.7 %
[3]	PZT	disk	6.8 mm diameter	0.75 mm	2.8	-	36.7 %
[44]	PZT	disk	15 mm diameter	3 mm	0.673	1000	27 %
[4]	PZT	disk	41.36 mm^2	-	1.2	-	50.4 %
[5]	PZT	block	1.7 mm^3	-	1	0.065	3.4 %
[6]	PZT	rectangular	1×1 mm^2	1.4 mm	1.3	0.6	63 %
[10]	AlN PMUT	rectangular array	8×8 mm^2	300 µm	2	0.001	-
[11]	AlN PMUT	disk	200×200 µm^2		1.7	0.085	0.12 %
[12]	AlN PMUT	rectangular array	2.5 mm^2	7.45 µm	3	0.019	0.236 %
[13]	PZT PMUT	rectangular array	2.058 mm^2		0.37	0.059	0.375 %
[14]	PZT PMUT	rectangular	2×2 mm^2	40 µm	0.088	0.7	0.33 %
[45]	AlScN PMUT	disk	12.25 mm^2	0.5 µm	0.7	1	8.1 %
[26]	Pre-Charged CMUTs	rectangular array	0.84×7.56 mm^2	700 µm	5.85	0.78	47 %
This work	Pre-Charged CMUTs	squared array	5×5 mm^2	700 µm	$1 - 2.4$	$16.6 - 66$ $6.9 - 41.5$	$15.5\,\% - 86.6\,\%$ (Conjugate Matching) $6.7\,\% - 54.5\,\%$ (No Matching)

case. However, at low frequency (1 MHz), the agreement between the simulations and experiments is less consistent for both charging fields, particularly in the *Conjugate Matching* case, where the measured efficiency is significantly lower than the simulated one. This discrepancy at low frequency can be attributed to the relatively high inductance values used, which are approximately an order of magnitude higher than those used for high-frequency matching. At these higher inductance values, the performance of commercial inductors is more affected by nonidealities and parasitic effects (e.g., lower self-resonance, higher equivalent series resistance (ESR), etc.). Moreover, during some experiments, we connected multiple inductors in series to achieve the correct inductance values, which may have further increased parasitic effects due to their interconnection.

Table IV shows the comparison of the results achieved in this work to the performance reported by other groups using PZT transducers and MUTs. The efficiency is calculated considering the total active receiver area, i.e., including the space between the active transducer elements. Our experiments yielded power conversion efficiencies within the range of, and often superior to, those obtained with PZT transducers, and significantly higher than those achieved with PMUTs. Even the lowest efficiency values from our experiments significantly exceeded those achieved with PMUTs. These lower values can be attributed to nonidealities in the components and experimental setup that are not taken into account in the model, as previously discussed. Additionally, our experiments demonstrated that even without using a matching inductor, we achieved efficiencies comparable to the values reported in Table IV. These results are significantly given the challenges associated with using an inductor in an IMD or integrating a CMUT onto an ASIC.

In general, it is advantageous to operate at the frequency at which the phase is minimum, whether a matching network is used or not. When using matching networks, where ideally the CMUT reactance can be completely compensated around a selected frequency, operating at the minimum phase frequency provides the maximum power bandwidth and consequently greater tolerance to variability of any of the parameters. In the absence of a matching network, it is also convenient to operate at the minimum phase frequency, as it corresponds to the condition of the lowest reactance-to-resistance ratio, resulting in maximum power transfer to an optimal load and thus maximum efficiency. In addition, when using a matching network, it is beneficial if the series resistance of the electrical interconnections is small compared to the CMUT's real part of the impedance and to use inductors with low ESR. R_s, in fact, limits the current flowing from the inductor toward the equivalent capacitive reactance, decreasing its efficiency in compensating the capacitive part. In addition, the matching inductor itself is not an ideal component having its own parasitic series resistance. Finally, the interconnection's series resistance as well as the inductor's ESR may significantly affect the efficiency to such an extent that beyond certain values, it is preferable to operate without matching networks.

Varying the built-in bias voltage by charging the devices at different electric fields allows shifting the frequency at which their phase is minimum to higher or lower values. However, it does not impact the minimum phase value [Fig. 6(b)]. For higher charging fields, the impedance magnitude is lower, resulting in better matching to low impedance loads, which can be advantageous depending on the load voltage and current requirements. However, it must be considered that the ratio between the real part of the impedance and the series resistance becomes less favorable, causing a decrease in efficiency. Another advantage of lowering the impedance magnitude is that smaller inductance values and thus also physically smaller inductors are needed for matching, which can be relevant if space constraints exist. Moreover, higher charging fields allow for greater dynamic ranges, as the CMUT is biased in deeper collapse, farthest from the snapback condition, thus allowing higher RX pressure operation. On the other hand, choosing a higher charging field, and therefore a higher minimum phase frequency, must be done with the consideration of the application and the propagation medium.

The latter determines the power loss between the transmitter and receiver. For example, within the body at a distance of 10 cm between the transmitter and receiver, using an operating frequency of 2.4 MHz results in 0.9 dB more attenuation at the receiver compared to 1 MHz. Therefore, in such cases, selecting a lower frequency might be advantageous despite the need for a larger matching inductor.

Finally, given that in these experiments we used about half of the maximum allowed ultrasound intensity for safe in-body use [36], the power at the load is in the range of values required by IMDs. Although, in these experiments, we considered simplified scenarios in terms of the type of matching circuit, choosing a matching type that satisfies the current and voltage requirements of a real application load is not expected to significantly change the performance.

Ultimately, since the performance of different device variants is comparable when connected to an optimally matched load, future optimization efforts will focus on improving charge retention over time, although for certain applications, such as disposable devices used in short-term or acute settings, the existing charge retention levels are already sufficient. As previously discussed, Si_3N_4 has a higher charge-trapping capacity compared to Al_2O_3, yet their overall charge retention performance is similar, with minimal differences observed between the two materials. However, from a manufacturing perspective, Si_3N_4 has notable advantages. Its deposition is achieved using PECVD, which is significantly faster than the ALD process required for Al_2O_3. This faster deposition process makes Si_3N_4 a more suitable choice for high-volume production. Additionally, the transport mechanism in Si_3N_4 is charge-based and well-documented in the literature, providing a solid foundation for further optimization.

IV. Conclusion

In this article, we investigated the performance of pre-charged collapse-mode CMUTs as ultrasonic receivers in wireless power transfer for IMDs. We presented a low-temperature, sacrificial release-based microfabrication technology for collapse-mode CMUTs that was modified to introduce a charge-storage dielectric layer to provide a built-in bias, thereby eliminating the need for an external high-voltage generator. We fabricated CMUT prototypes using two different charge storage materials, specifically PECVD Si_3N_4 and ALD Al_2O_3, and investigated the effect of the dielectric thickness separating them from the conductive electrode. The fabricated prototypes were pre-charged at different electric fields and characterized by I–V and CV measurements to evaluate the effective bias point. Their charge retention was assessed through electrical stress tests supported by electrical impedance measurements. We, then, analyzed the performance of the realized prototypes using both simulations and measurements to evaluate the power conversion efficiency to an optimal load as a function of bias condition and operating frequency, with or without electrical matching. Simulations, based on accurate equivalent circuit modeling with parameters fit from impedance measurements, allowed us to analyze the effect of parasitic series resistance on efficiency and to interpret the experimental power conversion results. We observed and discussed how the highest efficiencies can be obtained under CMUT precharging with the highest electric fields and at higher frequencies, and highlighted the extent to which the effect of series resistance can limit the efficiency. The measurements showed efficiencies up to 54.5% and 86.6% under no matching and conjugate matching conditions, respectively. The achieved efficiencies are significantly higher than other MUTs reported in the literature and comparable or superior to those obtained with state-of-the-art conventional bulk piezoelectric transducers.

The results of this article demonstrate that pre-charged collapse-mode CMUT is a promising technology for high-performance, integrated, lead-free transducers suitable for IMDs and systems. This technology is also promising for applications where the need for externally supplied high bias voltages is a critical limiting factor, such as ultraportable ultrasound imaging systems, wearable devices and patches, intravascular or intracardiac ultrasound catheters, or even for neuromodulation, thanks to the design freedom and modularity of this CMUT platform.

Appendix

To determine the optimal load in the case without matching, we derived the maximum power transfer condition for a generator with a complex equivalent source impedance and a purely resistive load. Consider a voltage generator V_e with an equivalent series source impedance $Z_e = R_e + jX_e$. When the load Z_L is purely resistive, $Z_L = R_L$, the power transferred to the load is expressed as

$$\begin{aligned} P_L &= |I_L|^2 \cdot R_L \\ &= \frac{|V_e|^2}{|Z_e + R_L|^2} \cdot R_L \\ &= \left| \frac{V_e}{(R_e + R_L) + jX_e} \right|^2 \cdot R_L \\ &= \frac{|V_e|^2 \cdot R_L}{(R_e + R_L)^2 + X_e^2} \end{aligned} \tag{3}$$

where I_L is the current through the load resistor R_L. To maximize P_L, we differentiate P_L with respect to R_L and set the derivative equal to zero

$$\frac{dP_L}{dR_L} = \frac{|V_e|^2\left[(R_e + R_L)^2 + X_e^2 - 2R_L(R_e + R_L)\right]}{\left[(R_e + R_L)^2 + X_e^2\right]^2} = 0. \tag{4}$$

Simplifying this equation gives

$$(R_e + R_L)^2 + X_e^2 - 2R_L(R_e + R_L) = 0 \tag{5}$$

which reduces to

$$R_L^2 = R_e^2 + X_e^2. \tag{6}$$

Therefore,

$$R_L = \sqrt{R_e^2 + X_e^2} = |Z_e|. \tag{7}$$

This result shows that the value of R_L that maximizes the power transferred to the load is indeed the magnitude of the source impedance, $|Z_e|$.

ACKNOWLEDGMENT

The authors would like to thank Eugene Timmering for the fabrication of the CMUT devices, Bart Mos for the help with the acoustic measurements, Paul Dijkstra and Jacco Scheer for the assembly of the CMUTs on PCBs, and Wouter Dekkers for the 3-D printing of the pieces of the experimental setup.

Marta Saccher is with the Department of Microelectronics, Faculty of Electrical Engineering, Mathematics and Computer Science, Delft University of Technology, 2628 CD Delft, The Netherlands (e-mail: m.saccher@tudelft.nl).

Alessandro Stuart Savoia is with the Department of Industrial, Electronic, and Mechanical Engineering, Roma Tre University, 00146 Rome, Italy (e-mail: alessandro.savoia@uniroma3.it).

Rob van Schaijk and Johan H. Klootwijk are with the MEMS and Micro Devices Department, Philips Engineering Solutions, 5656 AE Eindhoven, The Netherlands.

Ronald Dekker is with the Department of Microelectronics, Faculty of Electrical Engineering, Mathematics and Computer Science, Delft University of Technology, 2628 CD Delft, The Netherlands, and also with the MEMS and Micro Devices Department, Philips Engineering Solutions, 5656 AE Eindhoven, The Netherlands.

REFERENCES

[1] A. Lowe and N. V. Thakor, *The 2020 Roadmap for Bioelectronic Medicine*. Singapore: Springer, 2023, pp. 3407–3445.

[2] S. H. Song, A. Kim, and B. Ziaie, "Omnidirectional ultrasonic powering for millimeter-scale implantable devices," *IEEE Trans. Biomed. Eng.*, vol. 62, no. 11, pp. 2717–2723, Nov. 2015.

[3] H. S. Gougheri, A. Dangi, S.-R. Kothapalli, and M. Kiani, "A comprehensive study of ultrasound transducer characteristics in microscopic ultrasound neuromodulation," *IEEE Trans. Biomed. Circuits Syst.*, vol. 13, no. 5, pp. 835–847, Oct. 2019.

[4] Y. Shigeta, Y. Hori, K. Fujimori, K. Tsuruta, and S. Nogi, "Development of highly efficient transducer for wireless power transmission system by ultrasonic," in *IEEE MTT-S Int. Microw. Symp. Dig.*, May 2011, pp. 171–174.

[5] D. K. Piech et al., "A wireless millimetre-scale implantable neural stimulator with ultrasonically powered bidirectional communication," *Nat. Biomed. Eng.*, vol. 4, no. 2, pp. 207–222, 2020.

[6] J. Charthad, M. J. Weber, T. C. Chang, and A. Arbabian, "A mm-sized implantable medical device (IMD) with ultrasonic power transfer and a hybrid bi-directional data link," *IEEE J. Solid-State Circuits*, vol. 50, no. 8, pp. 1741–1753, Aug. 2015.

[7] J. Charthad et al., "A mm-sized wireless implantable device for electrical stimulation of peripheral nerves," *IEEE Trans. Biomed. Circuits Syst.*, vol. 12, no. 2, pp. 257–270, Apr. 2018.

[8] H. Jaffe, "Piezoelectric ceramics," *J. Amer. Ceram. Soc.*, vol. 41, no. 11, pp. 494–498, Apr. 1958.

[9] Y. Birjis et al., "Piezoelectric micromachined ultrasonic transducers (PMUTs): Performance metrics, advancements, and applications," *Sensors*, vol. 22, no. 23, p. 9151, Nov. 2022.

[10] B. Herrera, F. Pop, C. Cassella, and M. Rinaldi, "AlN PMUT-based ultrasonic power transfer links for implantable electronics," in *Proc. 20th Int. Conf. Solid-State Sensors, Actuat. Microsystems Eurosensors*, Jun. 2019, pp. 861–864.

[11] E. Mehdizadeh and G. Piazza, "AlN on SOI PMUTs for ultrasonic power transfer," in *Proc. IEEE Int. Ultrason. Symp. (IUS)*, Sep. 2017, pp. 1–4.

[12] Z. Rong, M. Zhang, Y. Ning, and W. Pang, "An ultrasound-induced wireless power supply based on AlN piezoelectric micromachined ultrasonic transducers," *Sci. Rep.*, vol. 12, no. 1, p. 16174, Sep. 2022.

[13] Q. Shi, T. Wang, and C. Lee, "MEMS based broadband piezoelectric ultrasonic energy harvester (PUEH) for enabling self-powered implantable biomedical devices," *Sci. Rep.*, vol. 6, no. 1, p. 24946, 2016.

[14] H. Basaeri, Y. Yu, D. Young, and S. Roundy, "A MEMS-scale ultrasonic power receiver for biomedical implants," *IEEE Sensors Lett.*, vol. 3, no. 4, pp. 1–4, Apr. 2019.

[15] K. K. Park, O. Oralkan, and B. T. Khuri-Yakub, "A comparison between conventional and collapse-mode capacitive micromachined ultrasonic transducers in 10-MHz 1-D arrays," *IEEE Trans. Ultrason., Ferroelectr., Freq. Control*, vol. 60, no. 6, pp. 1245–1255, Jun. 2013.

[16] A. Kshirsagar, A. Sampaleanu, R. Chee, W. Moussa, and R. J. Zemp, "Pre-charged CMUTs with efficient low-bias voltage operation for medical applications," in *Proc. IEEE Int. Ultrason. Symp. (IUS)*, Jul. 2013, pp. 1728–1730.

[17] M.-C. Ho, M. Kupnik, K. K. Park, and B. T. Khuri-Yakub, "Long-term measurement results of pre-charged CMUTs with zero external bias operation," in *Proc. IEEE Int. Ultrason. Symp.*, Oct. 2012, pp. 89–92.

[18] K. K. Park, M. Kupnik, H. J. Lee, O. Oralkan, and B. T. Khuri-Yakub, "Zero-bias resonant sensor with an oxide-nitride layer as charge trap," in *Proc. IEEE Sensors*, Nov. 2010, pp. 1024–1028.

[19] F.-Y. Lin, W.-C. Tian, and P.-C. Li, "CMOS-based capacitive micromachined ultrasonic transducers operating without external DC bias," in *Proc. IEEE Int. Ultrason. Symp. (IUS)*, Jul. 2013, pp. 1420–1423.

[20] W. Y. Choi, C. H. Lee, Y. H. Kim, and K. K. Park, "Comparison of Si_3N_4-SiO_2 and SiO_2 insulation layer for zero-bias cmut operation using dielectric charging effects," *IEEE Trans. Ultrason., Ferroelectr., Freq. Control*, vol. 67, no. 4, pp. 879–882, Apr. 2020.

[21] M. Annayev, F. Y. Yamaner, and O. Oralkan, "A pre-charged CMUT structure with a built-in charge storage capacitor," in *Proc. IEEE Int. Ultrason. Symp.*, Oct. 2022, pp. 1–3.

[22] H. Martinussen, A. Aksnes, and H. E. Engan, "Investigation of charge diffusion in CMUTs using optical interferometry," in *Proc. IEEE Ultrason. Symp.*, Nov. 2008, pp. 1218–1221.

[23] K. Midtbo and A. Ronnekleiv, "Analysis of charge effects in high frequency CMUTs," in *Proc. IEEE Ultrason. Symp.*, Nov. 2008, pp. 379–382.

[24] L. L. P. Wong, S. Na, A. I. H. Chen, and J. T. W. Yeow, "A novel method for measuring dielectric charging of CMUT arrays," in *Proc. IEEE Int. Ultrason. Symp.*, Sep. 2014, pp. 185–188.

[25] R. Van Schaijk, M. I. T. Zandt, P. Robaeys, M. Slotboom, J. Klootwijk, and P. Bekkers, "Reliability of collapse mode CMUT," in *Proc. IEEE Int. Ultrason. Symp. (IUS)*, Sep. 2023, pp. 1–4.

[26] S. Kawasaki, Y. Westhoek, I. Subramaniam, M. Saccher, and R. Dekker, "Pre-charged collapse-mode capacitive micromachined ultrasonic transducer (CMUT) for broadband ultrasound power transfer," in *Proc. IEEE Wireless Power Transf. Conf. (WPTC)*, Jun. 2021, pp. 1–4.

[27] M. Saccher, S. Kawasaki, J. H. Klootwijk, R. Van Schaijk, and R. Dekker, "Modeling and characterization of pre-charged collapse-mode CMUTs," *IEEE Open J. Ultrason., Ferroelectr., Freq. Control*, vol. 3, pp. 14–28, 2023.

[28] S. Kawasaki, M. Saccher, W.-J. de Wijs, J. van Den Brand, and R. Dekker, "Ultrasound imaging with pre-charged collapse-mode CMUTs," in *Proc. IEEE Int. Ultrason. Symp. (IUS)*, Sep. 2023, pp. 1–4.

[29] M. Saccher et al., "A comparative study of Si_3N_4 and Al_2O_3 as dielectric materials for pre-charged collapse-mode CMUTs," in *Proc. IEEE Int. Ultrason. Symp. (IUS)*, Sep. 2023, pp. 1–4.

[30] M. Saccher, S. Kawasaki, and R. Dekker, "The long-term reliability of pre-charged CMUTs for the powering of deep implanted devices," in *Proc. IEEE Int. Ultrason. Symp. (IUS)*, Sep. 2021, pp. 1–4.

[31] W. P. Mason, *Electromechanical Transducers and Wave Filters*. New York, NY, USA: Van Nostrand, 1942.

[32] E. F. Arkan and F. L. Degertekin, "Analysis and design of high-frequency 1-D CMUT imaging arrays in noncollapsed mode," *IEEE Trans. Ultrason., Ferroelectr., Freq. Control*, vol. 66, no. 2, pp. 382–393, Feb. 2019.

[33] S. Butterworth, "On a null method of testing vibration galvanometers," *Proc. Phys. Soc. London*, vol. 26, no. 1, p. 264, 1913.

[34] K. Van Dyke, "The piezo-electric resonator and its equivalent network," *Proc. Inst. Radio Eng.*, vol. 16, no. 6, pp. 742–764, 1923.

[35] *FOCUS*. Accessed: Jun. 3, 2024. [Online]. Available: https://www.egr.msu.edu/~fultras-web/

[36] U.S. Food and Drug Administration. (2019). *Marketing Clearance of Diagnostic Ultrasound Systems and Transducers: Guidance for Industry and Food and Drug Administration Staff*. Accessed: Aug. 22, 2024. [Online]. Available: https://www.federalregister.gov/documents/2019/06/27/2019-13687/marketing-clearance-of-diagnostic-ultrasound-systems-and-transducers-guidance-for-industry-and-food

[37] J. T. Gaskins et al., "Review-investigation and review of the thermal, mechanical, electrical, optical, and structural properties of atomic layer deposited high-kdielectrics: Beryllium oxide, aluminum oxide, hafnium oxide, and aluminum nitride," *ECS J. Solid State Sci. Technol.*, vol. 6, no. 10, pp. 189–208, 2017.

[38] M. Pekař, W. U. Dittmer, N. Mihajlović, G. van Soest, and N. de Jong, "Frequency tuning of collapse-mode capacitive micromachined ultrasonic transducer," *Ultrasonics*, vol. 74, pp. 144–152, Feb. 2017.

[39] J. J. H. Gielis, B. Hoex, M. C. M. Van De Sanden, and W. M. M. Kessels, "Negative charge and charging dynamics in Al_2O_3 films on Si characterized by second-harmonic generation," *J. Appl. Phys.*, vol. 104, no. 7, 2008, Art. no. 073701.

[40] X. Zhang, B.-W. Liu, Y. Zhao, C.-B. Li, and Y. Xia, "Influence of annealing temperature on passivation performance of thermal atomic layer deposition Al_2O_3 films," *Chin. Phys. B*, vol. 22, no. 12, 2013, Art. no. 127303.

[41] Y.-S. Lee, Y.-H. Lee, H.-J. Ju, W.-J. Lee, H. S. Lee, and S.-K. Rha, "Characteristics of $SiO_2/Si_3N_4/SiO_2$ stacked-gate dielectrics obtained via atomic-layer deposition," *J. Nanosci. Nanotechnol.*, vol. 11, no. 7, pp. 5795–5799, 2011.

[42] S. Arra, J. Leskinen, J. Heikkila, and J. Vanhala, "Ultrasonic power and data link for wireless implantable applications," in *Proc. 2nd Int. Symp. Wireless Pervasive Comput.*, 2007, p. 1.

[43] S.-N. Suzuki, S. Kimura, T. Katane, H. Saotome, O. Saito, and K. Kobayashi, "Power and interactive information transmission to implanted medical device using ultrasonic," *Jpn. J. Appl. Phys.*, vol. 41, pp. 3600–3603, May 2002.

[44] S. Ozeri, D. Shmilovitz, S. Singer, and C. C. Wang, "Ultrasonic transcutaneous energy transfer using a continuous wave 650 kHz Gaussian shaded transmitter," *Ultrasonics*, vol. 50, no. 7, pp. 666–674, 2010.

[45] B. Herrera, P. Simeoni, G. Giribaldi, L. Colombo, and M. Rinaldi, "Scandium-doped aluminum nitride PMUT arrays for wireless ultrasonic powering of implantables," *IEEE Open J. Ultrason., Ferroelectr., Freq. Control*, vol. 2, pp. 250–260, 2022.

Marta Saccher (Member, IEEE) received the B.Sc. degree in biomedical engineering from the Polytechnic University of Milan, Milan, Italy, in 2017, and the M.Sc. degree (cum laude) in biomedical engineering and the Ph.D. degree (cum laude) in MEMS ultrasound from Delft University of Technology (TU Delft), Delft, The Netherlands, in 2019 and 2024, respectively.

During her Ph.D., she was a Guest Researcher with Philips, Eindhoven, The Netherlands. She is currently holding a scientist position at TNO, The Hague, The Netherlands, working on ultrasound for different applications.

Alessandro Stuart Savoia (Member, IEEE) received the Laurea (M.S.) and Ph.D. degrees in electronic engineering from Roma Tre University, Rome, Italy, in 2003 and 2007, respectively, and the National Scientific Qualification (ASN) for Full Professor in electronics, in 2020.

Since 2007, he has been holding a postdoctoral research position at the Department of Electronics Engineering, Roma Tre University. From 2008 to 2010, he participated, as a Co-Founder and a Research and Development Manager, in an academic spin-off company of Roma Tre University, focused on the industrial exploitation of MEMS-based ultrasonic transducers [capacitive micromachined ultrasonic transducer (CMUT)], leveraging scientific results achieved during his Ph.D. and postdoctoral research. In 2014, he became an Assistant Professor of electronics with the Department of Engineering, Roma Tre University. He leads research activities with the Acousto-Electronics Laboratory, Department of Industrial, Electronic, and Mechanical Engineering, Roma Tre University, in the field of ultrasonic transducers. He has authored or co-authored more than 120 articles in international journals and conferences, most of them published in IEEE TRANSACTIONS and IEEE Conference Proceedings, and five book chapters. He holds seven international patents. His research interests are mainly focused on the development and system integration of MEMS ultrasonic transducers [CMUT and piezoelectric MUT (PMUT)].

Dr. Savoia serves the IEEE UFFC Society as an Associate Editor for IEEE TRANSACTIONS ON ULTRASONICS, FERROELECTRICS, AND FREQUENCY CONTROL, a Guest Editor for IEEE OPEN JOURNAL OF ULTRASONICS, FERROELECTRICS, AND FREQUENCY CONTROL, the Chair for the TPC Group 5 "Transducers and Transducer Materials" of the International Ultrasonics Symposium, and an Elected Member for AdCom.

Rob van Schaijk was born in Schaijk, The Netherlands, in 1971. He received the master's degree in applied physics from the Technical University of Eindhoven, Eindhoven, The Netherlands, in 1995, and the Ph.D. degree in semiconductor physics from the University of Amsterdam, Amsterdam, The Netherlands, in 1999.

He has 20 years of experience in semiconductors, MEMS, and IC technology in different positions, from Senior Scientist to Research and Development Manager. From 1999 to 2007, he worked with Philips Research, Philips Semiconductors, Eindhoven, and NXP Semiconductors, Eindhoven, on topics around silicon processing. From 2007 to 2017, he worked as a Principal Researcher, a Program Manager, and a Research and Development Manager with the Holst Centre, IMEC, Leuven, Belgium, with a focus on the development of energy harvesters and sensors for use in wireless sensor nodes. In 2017, he joined the MEMS and Micro Devices Department, Philips Innovation Services, Eindhoven, as a Principal Architect. His main responsibility is MEMS process development with Philips MEMS Foundry, Eindhoven, with a focus on capacitive micromachined ultrasonic transducer (CMUT) technology. He has authored or co-authored over 100 publications and conference contributions, and holds more than 35 patents.

Johan H. Klootwijk (Senior Member, IEEE) received the M.Sc. and Ph.D. degrees in electrical engineering from the University of Twente, Enschede, The Netherlands, in 1993 and 1997, respectively.

He then joined the Philips Research Laboratories, Eindhoven, The Netherlands, where he has worked on a wide range of topics, a.o. wideband RF applications (a.o. Si, SiGe, and InP bipolar technologies), gas sensors, thin extreme ultraviolet lithography (EUV) membranes (pellicles) for the next-generation lithography tools, and wearable MEMS-based ultrasound patches. Since 1999, he has been a Senior Lecturer of semiconductor devices with the CTT Institute, Eindhoven, and the T2Prof Institute, Eindhoven. In 2021, he was appointed as Team Lead of the Ultra-Sound Applications Team, Philips Research, Eindhoven, working on digital ultrasound (US) solutions. In 2023, he moved to the Philips MEMS Foundry, Eindhoven, after the closure of Philips Research. In 2024, he was promoted to the grade of Principal Scientist. He has authored or co-authored over 80 scientific publications and conference contributions, and holds more than 25 U.S. patents.

Dr. Klootwijk received the Best Paper Award for his contribution to the ESSDERC Conference in 2001 and the Best Poster Award on the NATO-ASI Summercourse on ALD in 1995. For part of his work, he received the Bronze Award for the NXP Invention of the Year 2007 and the Bronze and Silver Invention Awards in 2015 and 2020, respectively. He served as the Tutorial Chairperson for the International Conference on Measurement and Teststructures (ICMTS) in 2002, 2008, 2011, and 2024, and the Technical Chairperson in 2014. As of 2025, the MEMS Foundry is continue as an independent company, named XIVER.

Ronald Dekker received the M.Sc. degree in electrical engineering from the Technical University of Eindhoven, Eindhoven, The Netherlands, and the Ph.D. degree from the Technical University of Delft, Delft, The Netherlands.

In 1988, he joined Philips Research, Eindhoven, where he worked on the development of RF technologies for mobile communication. Since 2000, his focus shifted to the integration of complex electronic sensor functionality on the tip of the smallest minimal invasive instruments such as catheters and guide wires. In 2007, he was appointed as part-time Professor with the Technical University of Delft, with a focus on organ-on-chip and bioelectronics medicines. Since 2013, he has been an initiator of a number of large European initiatives that all have in common the development of open technology platforms for electronic medical devices. He published in leading journals and conferences and holds more than 70 patents.